Published in final edited form as:
Anal Bioanal Chem. 2013 February ; 405(6): 1809–1820. doi:10.1007/s00216-012-6437-1.

Opportunities in multi dimensional trace metal imaging: Taking copper associated disease research to the next level

Stefan Vogt[1] and **Martina Ralle**[2,*]

[1]X-ray Science Division, Advanced Photon Source, Argonne National Laboratory, 9700 S. Cass Avenue, Argonne, IL 60439

[2]Department of Biochemistry and Molecular Biology, Oregon Health & Science University, 3181 SW Sam Jackson Park Rd, Portland, OR 97239

Abstract

Copper plays an important role in numerous biological processes across all living systems predominantly because of its versatile redox behavior. Cellular copper homeostasis is tightly regulated and disturbances lead to severe disorders such as Wilson disease (WD) and Menkes disease. Age related changes of copper metabolism have been implicated in other neurodegenerative disorders such as Alzheimer's disease (AD). The role of copper in these diseases has been topic of mostly bioinorganic research efforts for more than a decade, metal-protein interactions have been characterized and cellular copper pathways have been described. Despite these efforts, crucial aspects of how copper is associated with AD, for example, is still only poorly understood. To take metal related disease research to the next level, emerging multi dimensional imaging techniques are now revealing the copper metallome as the basis to better understand disease mechanisms. This review will describe how recent advances in X-ray fluorescence microscopy and fluorescent copper probes have started to contribute to this field specifically WD and AD. It furthermore provides an overview of current developments and future applications in X-ray microscopic methodologies.

Keywords

imaging; X-ray; fluorescence; copper; neurological disease

Introduction

Metals and their involvement in health and disease are of ever growing importance in biomedical research. Lighter elements such as Ca participate in complex signaling pathways that are still being unraveled while transition metals are often co-factors in proteins where they undergo chemical state alterations (i.e. redox reactions) in enzymatic reactions they facilitate. While the reactivity of metals is of great use for facilitating enzymatic reactions it also requires strict control to mitigate toxicity. Therefore, metal homeostasis is tightly managed by cells and any disturbance leads to severe consequences. A comprehensive metallomic study would typically entail choosing a pathway for a specific metal and then investigating metal concentration, distribution, and metal-protein binding as well as changes thereof in healthy and disease. While measuring bulk metal concentrations as well as exploring metal-proteins interactions employs established methods and instrumentation, reliable, user-friendly techniques to produce spatially resolved data of metal content in biological specimen have only largely emerged during the past 10 years. Examples are

*Corresponding author: rallem@ohsu.edu, Phone (503) 494-3441, Faxe (503) 494 8393.

synchrotron based X-ray fluorescence microscopy (XFM), fluorescent metal sensors, secondary ion mass spectrometry (SIMS) and nano-SIMS, laser ablation inductively coupled mass spectrometry (LA-ICPMS), electron probe X-ray micro-analysis (EPXMA) and proton-induced X-ray emission (PIXIE) (for a recent review on these methods and their application to metallomic studies in neurodegenerative diseases see [1]).

This report will review recent progress in the metallome of mammalian Cu with respect to unraveling the disease mechanisms of two human disorders: Wilson disease (WD) and Alzheimer's disease (AD). We will specifically discuss contributions to this field made by imaging techniques, predominantly XFM studies and fluorescent copper sensors. We will furthermore describe new methodologies and developments in X-ray fluorescence tomography, XFM imaging at the nanoscale, and provide a perspective on sample preparation.

Imaging methods

X-ray based microscopy

X-ray microscopy (XRM) and specifically synchrotron-based XRM methods are increasingly used either as stand-alone or in combination with other correlative techniques to image cellular, organelle, or elemental structures in biology. The advantage of using X-rays in biological imaging is based on their penetration debth which allows for imaging close or at the native state of cells or tissue rather than bulk or homogenized and fractionated samples. Advances in focusing optics now yield microscopes with 20 nm resolution while tomographic reconstructions enables 3-dimensional imaging. Some correlative approaches such as fluoresecent microscopy allow for targeting of regions of interest prior to measurement while others such as Fourier transform infrared micro spectroscopy (FTIRM) are used to complement XRM information with chemical properties.

Two main classes of X-ray microscopy outline the two major applications. Soft X-rays (2–5 nm wavelength) are used to measure the intrinsic phase contrast of lighter elements i.e. detecting cellular and intracellular structures such as organelles etc. Detection is made in transmission mode, the detector is located in line with X-ray and sample. Because of limited penetration of soft X-rays, samples have to be thin (~100 nm). Hard X-rays in combination with Zernike phase contrast techniques enable users to perform X-ray tomography on thicker samples (>10 μm). The resulting hard X-ray phase contrast images are often used in combination with X-ray fluorescence (XFM), a technique that will yield quantitative information with high spatial resolution about elemental distribution (see below).

Chemical state mapping (XANES)

XANES is an attractive method to gain information about an elements redox status when imaging biological material. To determine oxidation states of metals a stationary focused X-ray beam (usually 5 μm × 5 μm) is applied to a target cell or tissue samples and the absorption of X-ray photons is monitored while scanning the energy through the X-ray abosprtion edge of the element of choice. The position of the edge (its first inflection point) as well as the shape of the edge (specifically 'pre-edge features') contain information about the oxidation and often the coordination sphere. Data analysis is still almost exclusivly performed in an empiric manner by comparing experimental data with measured model compounds. Several groups have sucessfully determined the oxidation states of mostly Fe and Cu, in biological specimen [2–4] (for a recent review see Ortega et al. [5]). A nice example is a more recent publication by Glasauer et al. who studied the oxidation state of Fe in cytoplasmic granules in *Shewanella putrefaciens* that are formed during anaerobic respiration and found Fe to be in a mixed valence state [2]. Yang et al. determined the oxidation state of Cu in a mouse fibroblast cell line that had been exposed to 200 μM $CuCl_2$.

Their results indicated that copper is predominatly present as Cu(I) in a linear to trigonal coordination environment by mostly sulfur [4].

While the experimental setup and data analysis for XANES is straightforwar literature examples are still rare. Longer dwell times (sample remains stationary during a 5 – 10 min scan) with highly brilliant, focused X-rays induce significant photoreduction and radiation damage, XANES measurements have therefore carefully be evaluated. Lastly, even a small beamsize of 5 μm × 5 μm will contain multiple proteins and the resulting XANES spectrum will be a representation of the average oxidation state which is mostly likely dominated by a metals bound to a high abundance stoarage protein.

X-ray fluorescence microscopy (XFM)

XFM is part of the X-ray microscopy super group and is rapidly becoming the method of choice for an ever-growing community of bioanalytical researchers to probe trace elements in biological systems. It is used for both quantitative visualization as well as analysis of the local chemical state of elements of interest (for in depth reviews of XFM see [6,7,5,8–12]). Briefly, hard X-rays (≥10 keV), with an incident energy chosen to be above the relevant absorption edges of the elements of interest, are focussed onto the specimen, inner (K- or L-shell) electrons are knocked out, and the subsequent relaxation process causes the emission of X-ray fluorescence characteristic for the absorbing element. An energy dispersive detector system is usually used to record a full x-ray spectrum at each scan position and elemental maps for 10 or more chemical elements are then derived from these spectra. A scheme illustrating the experimental setup for XFM experiments is depicted in Fig. 1. The achievable spatial resolution is generally determined by the x-ray optics used, values that are routinely achieved today on a variety of instruments are in the micron range for Kirckpatrick-Baez mirror systems and on the order of 100's of nm for Fresnel zone plate based systems. Several systems have capabilities to achieve spatial resolutions well below 100 nm [12–14]. Recent years have not only seen significant improvements in X-ray optics development, but also in detector and data acquisition systems development, permitting, amongst other things, much more rapid data collection with significantly reduced overhead [15]. In terms of biological applications, XFM is a convenient probe to explore the elemental content in cells and tissue but it has also been shown to be a powerful tool in determining regulatory changes in cells and tissues. Chen et al. used XRF to confirm that cis-platin is sequestered in melanosomes in melanoma cells instead of nuclear targeting. The melanosomes were subsequently exported explaining the underlying mechanism of multidrug resistance in patients with melanoma [16]. Finney et al. demonstrated dynamic changes of the copper distribution in breast cancer cells. They found that copper relocates to the extracellular space during angiogenesis and based on these results suggested that copper plays has regulatory role in the process of angiogenesis.

XFM Imaging at the nanoscale and sample preparation—Several institutions are pursueing next generation X-ray fluorescence microprobes that enable imaging of trace metal content in biological systems at highest spatial resolution, in the range of 20–50 nm, with samples preserved as close as possible to the natural state. Radiation damage is generally manageable in X-ray fluorescence microscopy (dwell times are relatively short), its effects can, however, directly limit the achievable spatial resolution (see [17] for a discussion of the relation between required dose for imaging and structural damage to the sample). To mitigate the effects of radiation damage, the sample must therefore be adequatly preserved. While chemical fixation can work well for just structural studies it, often interferes with elemental content and can cause significant redistrubition of elements, in particular for diffusible ions[18,19]. The method of choice to preserve elemental content, such as the copper distribution, is cryo-fixation, preferably through plunge freezing

intoliquid nitrogen cooled liquid ethane (for thin samples) or high–pressure freezing for thick samples. This way vitrification is achieved without the creation of ice crystals that would damage the specimen structure. While subsequent freeze-drying and imaging of the sample at room temperature is a reasonable approach for investigations requireing moderate spatial resolution, freeze-drying does neither preserve the true 3D structure of the specimen well, nor does it preserve ultrastructure best. To make best use of the strengths of x-ray fluorescence microscopy, such as high penetration depth, a spatial resolution that is maintained through comparatively thick samples (as long as they are within the depth of focus of the used optics), and low background, but at the same time minimize self absorption artefacts for low-Z fluorescence, good samples thicknesses would then be on the order of 10 microns, well matched to typical cell sizes. To exploit the recent advances, and enable highest resolution trace metal mapping, several different approaches have been implemented. In vacuum-systems [13,20] have the advantage of minimized background and minimum absorption of low-Z elemental fluorescence, but require dedicated instrumentation. Approaches that work in ambient conditions permit more flexible use of the microprobe instrument but are not optimized for low Z element detection. One such approach is the use of a separated, cryo-cooled stage [12], another one is the use of a cryo-jet [21], similarily to methods in macromolecular crystallography.

Three-dimensional XFM—Since X-ray microprobes have a large depth of focus (≥100 μm), and the lateral spatial resolution does not deteriorate throughout the specimen, elemental maps acquired from the sample are projection images integrating the elemental content through the thickness of the sample, i.e. a three-dimensional object is projected into a two-dimensional plane. Interpretation of such an elemental map can be challenging, especially if the thickness exceeds more than one cell layer or at high spatial resolutions, because of multiple overlapping structures. In these cases it is desirable to visualize the elemental content of a sample in three dimensions (3D). When collecting data for 3D-XFM numerous projection images are acquired for different projection angles, to then reconstruct the full tomographic representation of the specimen. This technology is still facing some challenges with regards to routine implementation [22], but there have already been a number of impressive applications [23–25] and exciting advances have been made in recent years. An example is shown in Fig. 2, where De Jonge *et al.* visualized the 3D elemental distribution for the diatom *Cyclotella meneghiniana* as a proof-of-concept study. The authors achieved 400 nm resolution and were able to calculate concentrations for biologicaly relevant elements. The frustule is comprised of mainly Si, with less abundant Cu and Zn. P, K, and Ca were shown to accumulate in three distinct nuclei while Mn and Fe were shown to localize to ring shaped patterns around the diatom.

Several new or upgraded instruments are in various stages from conception, to implementation, to commissiong, to operation, promising the ability to image trace elemental content in frozen-hydrated biological specimens with spatial resolutions below 50 nm, in 3D. Several synchrotron radiation facilities have either come recently online or are in various stages of being built or upgraded, and offer valuable additional improvements in instrument performance through increased brightness and thereby focussed flux on the sample and corresponding improved throughput. These instrumentation advances, together with source and detector developments, as well as methods development such as the application of dose fraction approaches [26] towards XFM promise to enable full 3D visualization of trace elemental content of single cells [22]. Such advances will significantly improve our ability to investigate elements such as copper in biological systems close to their natural state within organelles, and enable new studies with potentially significant impact on our understanding of the multitude of roles that these elements play. [1]

Quantitation: XFM is inherently quantitative and application software developments allow users to quickly assess elemental concentrations in their samples [30,31]. Quantitation and concentration measurements with XFM are based on the fact that the X-rays penetrate the entire sample (typically in the range of 10 μm (high, sub-micron resolution) to 50 μm (low, micron resolution) thickness. Standard X-ray reference materials are used to correlate the fluorescent photon counts to area concentrations (μg/cm^2), though standard-less quantification is also possible. Resulting area concentrations are converted into volume concentrations if the thickness of the sample is known. If whole cells are imaged, elemental concentrations are often expressed as μg/cell.

Correlative techniques to complement XFM—XFM is based on the fluorescent emission of elements, and is particularly sensitive for heavier elements ($Z \geq 14$). As a consequence, cellular structures such as membranes cannot easily be recognized unless different cellular compartments contain substantially different amounts of one element. Nuclei, for example, can often be identified by the comparably higher abundance of phosphorous (Fig. 3). In order to co-localize elemental content with cellular sub structures such as organelles, XFM has to overcome the lack of contrast artificially by either applying other spectroscopic techniques to the same samples, making use of phase contrast [32–34], or by using appropriate biomarkers labeled with a heavy, non-physiologically relevant element. Miller et al. routinely employ Fourier transform infrared micro spectroscopy where the relative protein content of an area is determined by integrating the spectra from 1490 to 1580 cm^{-1}, the absorption range for the protein specific Amide II band. FTIRM measurements are carried out on the same samples after the XFM experiments [35–39]. McRae et al. used Fluoronanogold (FNG, [40,41]) where secondary antibodies carry a 1.4 nm Au-cluster in addition to a fluorophore. FNG labeled antibodies against mitochondria and the Golgi apparatus were visualized via the Au-cluster and subsequently co-localized with copper in the initial proof-of-concept study. Endres et al. showed how organic gadolinium MR probes can function as contrast agents for intracellular locations [42–44] while Paunesku et al. tracked the Ti signature from TiO_2 nancomposites that are used as intra cellular drug delivery vehicle [45,46]. Lastly, the European group of Corezzi et al. employed commercially available secondary CdSe/ZnS quantum dot antibodies against the human cancer marker Her2 and β-tubulin and followed the Se signature [47] in a cancer cell line. Another promising option for organelle labeling are Lanthanide (Ln^{3+}) containing conjugates for primary antibodies. Developed as markers for mass cytometry [48], Ln^{3+} ions (such as Pr^{3+}, or Sm^{3+}) consist of metal chelating polymers that are attached to primary antibodies via a reduced thiol group onto the Fc-fragment of the antibody (Fig. 4a). Each polymer carries about 30 Ln^{3+} ions and between 4 and 6 polymers are bound to one protein molecule. Therefore, a total of 120 – 130 Ln^{3+} ions are attached to each antibody. During the actual XFM experiment the Ln^{3+} distribution is monitored and co-localized with other metals of interest. The hypothetical application of these markers is illustrated in Fig. 4b–c. Fig. 4b) shows a false colored image of fibroblasts that labeled with DAPI (blue, nuclei) and anti-TG46, a marker for the *trans-Golgi* network (red). No information on the copper distribution is available. Fig. 4c) shows a hypothetical XFM map consisting of an overlay for the elements phosphorous (red, nuclei), copper (blue), and Pr (green, Pr-anti TG46 conjugate). A major advantage of this method is the convenient location of the Ln^{3+} L-edge's emission line. For Pr^{3+} or Sm^{3+}, for example this range is between 5 and 7 keV, which is well suited for typical XFM experiments where the maximum instrument

[1]One exciting development with regards to X-ray sources is the X-ray free electron laser (XEFLs). XEFLs produce X-ray pulses with peak intensities that are ~10^9 times more intense than synchrotron radiation [27]. The main application for XFELs is the determination of protein crystal structures from micro- or nano crystals [28,29]). As such (at least for now) XFELs is used to collect X-ray *diffraction* patterns and although one can imagine to one day collect absoprtion patterns in fluorescence or transmission mode with in x-y scanning mode this is as of yet not feasible.

sensitivity is just above the Zn Kedge (10 keV incident X-ray energy). Additionally, the use of a conjugated primary rather than a secondary antibody decreases the sample handling time and eliminates another source of non-specificity.

Fluorescent copper sensors

To monitor fluxes of labile copper in living systems several research groups developed copper sensitve fluorescent probes and sucessfully tested them on cells [49–52,4,53] and, recently, tissue [54]. Although the cytosolic levels of unbound copper are below 1 Cu per cell, the rapid rate by which this concentration can change suggests that part of this copper is easily accessible. The cytosolic Cu concenration in fibroblasts, for example, increases 3-fold or 10-fold when the growth medium is supplemented with with 100 μM copper for 4 or 48 hrs, respectively, (Ralle et al., unpublished results). Cu-fluorescent sensors are usually membrane permeable probes that consist of two π electron systems (a Cu-binding moiety and a fluorophore) separated and thus electronically disconnected by a short alkyl chain linker. In the unbond state the fluorescence is quenched by fast photo induced-electron transfer (PET) from or to the flourophore. Upon Cu binding the redox properties of the binding unit are altered. The PET process is slowed or stopped and thus enabling flourescent emssion [55]. Early probes were hampered by their lack of sensitivity and Fahrni et al. showed that the flourescent recovery upon Cu(I) binding can be incomplete due to ternary quenching pathways. His group subesequently adressed this and developed a high contrast probe in which the flourescent enhancement upon saturation is greater than 200-fold compared to a 5-fold increase of his earlier probes [4,56,57]. These probes, however, have so far not been tested in in vivo systems. C. Chang's group recently published the synthesis and application of a copper sensor (CS790) with an near infrared emission at 790 nm. The 15-fold fluoresent enhancement of his probe was sufficient to monitor labile copper in $Atp7b^{-/-}$ mice (see below and [54]).

The copper metallome

Copper is an essential trace element important in numerous biological processes. Its small electrochemical half cell potential (Cu(II)/Cu(I) = 150 mV, 300 – 550 mV in proteins [58]) makes it a versatile tool in enzymatic reactions including electron transfer or redox chemistry. This versatility also renders unbound or 'free' Cu a potential hazard. It promotes the formation of reactive oxygen species (ROS) such as hydroxyl radicals via electron abstraction from H_2O_2 [59]. Copper levels are tightly regulated to support physiological requirements and prevent buildup of toxic levels; the cellular content of 'free' copper is held to less than one Cu per cell [60,61]. Any disturbances in this regulatory process lead to severe consequences. Wilson and Menkes disease are directly caused by copper accumulation or deficiency, respectively, through inactivation of the copper exporting P_{1B} type ATPases ATP7b (Wilson disease) and ATP7a (Menkes disease) [62,63]. The association of copper in neurodegenerative diseases has been discussed in a plethora of papers (for a recent comprehensive review see [64]).

Copper binding proteins can be divided in two major classes, those which use copper for specific functions (copper enzymes, class (I)) and those which facilitate copper transport, transfer, and storage (class II) [65,58]. The sophisticated pathways for the latter class have been extensively studied in both eucaryotic and procaryotic systems and are described in several reviews [60,66,65,67]. It was further shown that the regulation of copper and iron (at least in mammals) are intertwined [68]. While research over the past 20 years has greatly advanced our knowledge of copper proteins and its pathways, disease related changes in these pathways remain largely elusive. This is in part also why it remains unclear how copper is associated with neurodegenerative diseases, for example Alzheimer's disease, as these are not caused by or involve a singular copper protein. The more general but

nonetheless complex question of how non-genetic causes and disturbances in copper regulation and pathways contribute to ailments such as cancer, Alzheimer's disease, or inflammation remains unanswered. Research targeting this question has to include a global approach: changes in organ, cellular, and intracellular copper distribution, concentration, and chemical state have to be considered. Bioanalytical sciences have to transition from a one-dimensional, protein specific, approach to a two- and three- dimensional approach. This review will describe research advances for the copper metallome as a consequence of developments in metal multi-dimensional imaging methods. We will focus on Wilson disease and Alzheimer's disease, two neurodegnerative disease of substantially different origin.

Copper homeostasis in Wilson and Menkes disease

Wilson disease (WD) is a genetic disorder of copper metabolism associated with severe hepatic, neurological, and psychiatric abnormalities. A major hallmark of WD in patients is the accumulation of copper in liver and frequently, basal ganglia. The affected gene, *ATP7B*, which encodes a copper transporting ATPase was identified in 1993 [69,62]. The protein, ATP7b, has been extensively studied [70,67]. Under basal copper conditions it localizes to the TGN and transports copper across the membrane to be incorporated into ceruloplasmin[71]. Upon elevation of intra cellular copper levels ATP7b relocates into vesicles close to the apical membrane and for biliary excretion [72,73]. ATP7b is the only known hepatic copper exporter and consequently its inactivation leads to accumulation of copper. WD can present with a clinical syndrome indistinguishable from chronic hepatitis or advanced cirrhosis of other origin [74]. The only reliable biochemical indicator of WD is greatly elevated copper in liver biopsy samples (> 250 μg/g dry tissue weight compared to 20–50 μg/g dry weight in control [75,76]). However, the level of copper *per se* does not correlate with either stage or severity of the disease. Genetically engineered *ATP7b null* mice confirmed the complex genotype - phenotype relationship [77–79]: It was shown that the *knock-out* mice do not start to exhibit substantial cellular damage until *after* the copper levels had peaked at 6 weeks of age. Significant changes in morphology are typically not observed until 12 weeks of age. In Menkes disease (MD), an x-linked genetic disorder, newborns are incapable of absorbing copper from the small instestines therefore developing a copper difficieny. The defective protein in MD, ATP7a, has >40% sequence identity with ATP7b and is expressed in most cells with the notable exception of hepatocytes[80,63]. Similar to ATP7b, ATP7a resides in the TGN at basal copper levels and relocates to the proximity of the basolateral membrane to aid in copper export when levels are elevated [81]. Because ATP7a plays a critical role in copper uptake from the small intestines, its dysfunction will lead to severe copper deficiency and usually death at the age of 3.

Elucidating the copper metallome for WD

Histological copper staining of liver sections from WD patients showed accumulated copper in the periportal regions in the earlier stages of the disease while at later stages copper was diffusely distributed in each lobule [82,83]. Other groups suggested that the intra-cellular localization of copper changes from mainly cytosolic copper in the early disease stages to predominantly lysosomal and nuclear at the later stages [84–86]. However, it was shown that histological stains for copper are unreliable, it appears that they only detect unbound or loosely bound copper [1,9]. In recent years researchers have utilized ATP7b null and control mice which greatly increased the sampling size and ensured a controlled environment.

Using XFM, Ralle at al. proposed a mechanism for copper accumulation that could explain the delayed onset of morphological changes in ATP7b$^{-/-}$ livers [87]: In the initial stages of WD massive amounts of copper enter the hepatocytes. Excess copper also enters the nucleus and triggers changes in the transcriptome. Later, copper recedes from the nucleus and other

compartments (including the cytosol) and becomes concentrated in deposits. This copper re-distribution (possibly into the lysosomes) was proposed as a self-protection mechanism of the cell against copper toxicity. Hirayama et al. demonstrated the ability of a fluorescent sensor, CS790, to monitor labile copper pools in cells and living mice, including the ATP7b$^{-/-}$ mice [54]. After testing the membrane permable version of CS790 on Hek293T cells (CS790-AM), Hirayama et al. injected mice (ATP7b$^{-/-}$ and *wild-type* controls) with 100 μM $Cu(Cl)_2$ solution 2 hrs prior to injection of CS790-AM and monitored the resulting increase in fluorescence caused by copper binding to the sensor. As expected they found copper predominantly accumulating in the liver of the mice with a higher fluorescent signal indicating a higher copper concentration originating from the *knock-out* mice livers. The authors also showed that upon administration of the copper chelator, ATN-224, a compound that is currently discussed as treatment for WD, the fluorescent signal (radiant efficiency) decreased by a factor of 2–3. A similar study by Peng et al. who used positron emission tomography to track ^{64}Cu in Atp7b$^{-/-}$ and wild type controls [88]. Similar to Hirayama et al. Peng et al. demonstrated the liver to be the major site of copper accumulation with impaired clearance for the *knock-out* mice (0.8 hrs versus 2.5 hrs of mean residence time for hepatic copper in *wild-type* compared to *null* mice). In addition, they reported an inital increase in clearance of copper from the kidney's, an organ where both ATP7a and ATP7b are expressed. They argued that in the absence of ATP7b ATP7a translocated from the basolateral to the apical membrane in a compensatory mechanism to relieve the increased burden of copper in the blood. Peng et al. were also able to monitor diffuse copper distribution in the intestines 2 hrs post injection with ^{64}Cu which could either be due to a higher sensitivity or better resolution of the PET images (pixel size ~100 μm). The major difference between these two studies are the timepoints. Peng et al. monitored Cu distribution starting immedeately post injection with 2 additional time points at 2 and 24 hrs post injection, Chang et al. only monitored one time point at 2 hrs post injection. Regardless, both studys represent the first examples of determining copper distributions in WD *knock-out* mice in vivo with sufficiently high spatial resolution. One possible future application for copper sensors is the localization of tumors in vivo as they show increased copper uptake. Patient would be injected with a copper containing solution and the distribution of copper would be subesequently monitored.

Another protein important to understand the involvement of copper that plays a crucial in WD and MD is Atox1, the copper chaperone that delivers Cu^+ to ATP7a and ATP7*b*[89–91]. Atox1 binds Cu^+ in the same linear Cys-Cu-Cys fashion as the N-terminal binding regions of Atp7a and Atp7b [92–94]. McRae et al. used SXRF to determine the distribution of Cu in an Atox1 deficient fibroblasts compared to wild type cells when exposed to 50 μM copper [95]. They reported that while copper preferrably localized to the peri-nuclear region in Atox1$^{+/+}$ cells it was diffusly distributed throughout the cell Atox1$^{-/-}$ cell. They also found that the copper concentration in Atox1$^{-/-}$ cells is about 1.5 × higher than in Atox1$^{+/+}$ cells when grown in basal conditions. Their results further underscored that Atox1 plays a significant role in maintaining proper cellular copper distrbution.

Copper in Alzheimer's disease

Alzheimer's disease (AD) is a progressive neurological disorder associated with extracellular amyloid-β (Aβ) deposits, A peptide oligomerization, intracellular neurofibrillary tangles (NFTs), synaptic toxicity, and oxidative stress. Although most of these processes or effects are understood individually, their complex, synergistic causes and consequences remain unclear.

A potential role of dyshomeostasis of metals was first proposed more than 60 years ago when Goodman et al presented a role for iron in AD [96]. Goodman saw elevated Prussian Blue staining (a histological stain for iron) in post-mortem tissues from AD cases. Since

then numerous papers and reviews have been published about a possible involvement of metals in AD (for more in-depth reviews see [97,1,47,98]).*Metallomics* recently dedicated an entire issue to the role of metals in neurodegenerative disorders[64]. Iron, copper, and zinc have been identified to play a role in the mechanics of Aβ oligomer formation[99,100,98], they have been found in plaques and NFT's[98], and are believed to be responsible for the widely observed oxidative stress in AD[101]. Despite this wealth of studies much controversy exists about the *specific* role of metals, particularly copper, in key processes in AD, and how global changes in copper concentration affect progression of the disease. Even basic questions such as whether brains of AD individuals exhibit elevated copper levels or rather a deficiency compared to healthy controls is subject of discussion and controversy. Much of this is due to the complexity of the problem: the brain is a heterogeneous organ and changes metal concentration will most likely be localized rather than global. Analyzing 'local' metal concentrations with reasonable resolution (≤1μm × 1μm) across an entire human brain is time consuming, let alone performing an longitudinal study of disease and control brains. Schrag et al. performed a meta-analysis of quantitative studies for Fe, Zn, and Cu in neo-cortical brain regions in post-mortem human tissue [102]. The authors concluded that neither Fe nor Zn were elevated and that Cu was in fact decreased in AD subjects which is somewhat contradicting the conclusion of one of the most cited review articles in AD-metal research by Bush who suggested a consensus in the literature for elevated metal concentrations in brain of AD patients [103]. Schrag et al. found that popular cited primary studies were qualitative, semi-quantitative (i.e. used metal to protein ratios as quantitation), or used tissue unsuited for quantitative analysis.

This is also true when trying to define the role of metals at the protein level: Simple models have proven to be a lot more complicated than in vitro analysis suggested. Tougu et al. examined the interaction of Cu(II) and Zn(II) with Aβ and subsequent oligomer and fibril formation[104]. He outlines the complexity and dependency of reaction conditions used when examining the role of Cu and Zn in AD. Tougu et al. concluded that both Cu and Zn enhance as well as inhibit the formation of Aβ fibrils.

Significant progress to elucidate the role of copper (and other metals) in AD was made by spatially resolved, multi dimensional techniques. Several studies determined the copper content in Aβ deposits (plaques). Lovell et al. found 1.5-fold elevated levels for copper in plaques when compared to neuropil from human AD subjects using particle induced X-ray emission (PIXE) [105]. Hutchinson et al. used LA-ICPMS on sections derived from a transgenic mouse model [106] and confirmed that copper was elevated in plaques (~4-fold). To identify Aβ deposits and correlate them with copper content, the mouse sections were stained with a Eu or Ni conjugated antibody. Similar to Lovell et al. the imaged sections were fixed in paraformaldehyde somewhat questioning the accuracy of the results as formalin fixation can significantly alter metal concentration and distribution in tissue [18]. L. Miller et al. performed the first spatially resolved study of copper levels in Aβ deposits from human plaques using cyro-fixed tissue [38,35]. They used a combination of FTIRM and XFM on thioflavin stained sections and were able to show that copper was 1.8-fold elevated in human Aβ deposits. The first quantitative imaging study on cryo-fixed, *unstained* Aβ plaques was performed by Rajendran et al. [107]. Similar to Lovell et al [105], the authors used PIXE for trace copper quantitation in plaques from brains of transgenic mice, however, instead of visualizing plaques by histochemical stains they performed scanning transmission microscopy Rutherford backscattering for structural characterization i.e. to identify Aβ deposits. Their results confirmed elevated copper (and iron and zinc) content in Aβ deposits.

Other imaging studies have been performed to determine the copper distribution, concentration, and longitudinal changes during disease progression. Similar to the one-

dimensional analysis of bulk tissue these studies were not always in agreement. In his initial PIXE study in 1998,Lovell et al. found 5-fold elevated copper in the neuropil for AD subjects compared to controls, (19 μg/g compared to 4 μg/g). A recent study by Wang et al. used cryo-fixed, unstained brain sections from a transgenic mouse model to investigate the copper distribution during disease progression [108]. The imaging method used was XFM with low resolution optics (scans were performed at 3 μm × 3 μm, and 60 × 60 μm resolution, respectively). The authors state that the copper levels in the hippocampus increased from 1 month of age to 18 months from 5 μg/g to 16 μg/g (no standard deviations were given) for the transgenic mice compared to 12 μg/g of Cu in 18 month old control mice. The opposite was found in the thalamus (20 μg/g in transgenic versus 60μg/g in control mice). The authors did not explain how they identified the hippocampus or the thalamus in their brain sections and it seem likely that areas that are known to be higher in copper (such as the peri-ventricular areas) were accidently included in some of the calculations. XFM experiments from our lab that also used a transgenic mouse model did not result in elevate copper content of the hippocampus, however, we did see a moderate increase in copper concentration from pre-symptomatic (5μg/g) to symptomatic mice (7 μg/g) [unpublished results].

Conclusions

Multi dimensional, high resolution imaging methods are beginning to elucidate the metallome of copper and its changes during diseases processes. Particularly, XFM methods are rapidly evolving in terms of resolution, three dimensional capabilities, and user accessibility and publications from the past 6 years have established central role for XFM in metallomic research. The involvement of copper in complex disorders like AD can only be determined by taking this research to the next level, i.e. from one to two or three dimensions. In combination with correlative techniques such as copper sensing fluorescent probes or lower resolution techniques such as LA-ICPMS, XFM will likely become the method of choice in the future to study copper pathways in biological systems.

Acknowledgments

The authors would like to gratefully acknowledge the use of the facilities at the Advanced Photon Source. This work was supported by the National Institutes of Health Grant GM090016 to MR, the use of the Advanced Photon Source was supported by the U.S. Department of Energy, Office of Science Contract DE-AC-02-6CH11357.

Abbreviations

WD	Wilson disease
AD	Alzheimer's disease
XFM	X-ray fluorescence microscopy
SIMS	secondary ion mass spectrometry
LA-ICPMS	laser ablation inductively coupled mass spectrometry
EPXMA	electron probe X-ray micro analysis
PIXIE	proton induced X-ray emission
FTIRM	Fourier transform infrared micro spectroscopy
amyloid-β	Aβ
NFT	neurofibrillary tangles

FGN Fluoronanogold

References

1. Bourassa MW, Miller LM. Metal Imaging in Neurodegenerative Diseases. Metallomics. 2012
2. Glasauer S, Langley S, Boyanov M, Lai B, Kemner K, Beveridge TJ. Mixed-valence cytoplasmic iron granules are linked to anaerobic respiration. Appl Environ Microbiol. 2007; 73(3):993–996.10.1128/AEM.01492-06 [PubMed: 17142380]
3. Kemner KM, Kelly SD, Lai B, Maser J, O'Loughlin EJ, Sholto-Douglas D, Cai Z, Schneegurt MA, Kulpa CF Jr, Nealson KH. Elemental and redox analysis of single bacterial cells by x-ray microbeam analysis. Science. 2004; 306 (5696):686–687. [PubMed: 15499017]
4. Yang L, McRae R, Henary MM, Patel R, Lai B, Vogt S, Fahrni CJ. Imaging of the intracellular topography of copper with a fluorescent sensor and by synchrotron x-ray fluorescence microscopy. Proc Natl Acad Sci U S A. 2005; 102(32):11179–11184. 0406547102 [pii]. 10.1073/pnas.0406547102 [PubMed: 16061820]
5. Ortega R, Deves G, Carmona A. Bio-metals imaging and speciation in cells using proton and synchrotron radiation X-ray microspectroscopy. J R Soc Interface. 2009; 6(Suppl 5):S649–658. rsif.2009.0166.focus [pii]. 10.1098/rsif.2009.0166.focus [PubMed: 19605403]
6. Fahrni CJ. Biological applications of X-ray fluorescence microscopy: exploring the subcellular topography and speciation of transition metals. Curr Opin Chem Biol. 2007; 11(2):121–127. S1367-5931(07)00033-6 [pii]. 10.1016/j.cbpa.2007.02.039 [PubMed: 17353139]
7. Paunesku T, Vogt S, Irving TC, Lai B, Barrea RA, Maser J, Woloschak GE. Biological applications of X-ray microprobes. Int J Radiat Biol. 2009; 85(8):710–713. 913458303 [pii]. 10.1080/09553000903009514 [PubMed: 19637082]
8. Lobinski R, Moulin C, Ortega R. Imaging and speciation of trace elements in biological environment. Biochimie. 2006; 88(11):1591–1604. S0300-9084(06)00236-7 [pii]. 10.1016/j.biochi.2006.10.003 [PubMed: 17064836]
9. Ralle M, Lutsenko S. Quantitative imaging of metals in tissues. Biometals. 2009; 22(1):197–205.10.1007/s10534-008-9200-5 [PubMed: 19130257]
10. Jensen MP, Aryal BP, Gorman-Lewis D, Paunesku T, Lai B, Vogt S, Woloschak GE. Submicron hard X-ray fluorescence imaging of synthetic elements. Anal Chim Acta. 2012; 722:21–28. S0003-2670(12)00254-1 [pii]. 10.1016/j.aca.2012.01.064 [PubMed: 22444530]
11. Paunesku T, Vogt S, Maser J, Lai B, Woloschak G. X-ray fluorescence microprobe imaging in biology and medicine. J Cell Biochem. 2006; 99(6):1489–1502.10.1002/jcb.21047 [PubMed: 17006954]
12. Bohic S, Cotte M, Salome M, Fayard B, Kuehbacher M, Cloetens P, Martinez-Criado G, Tucoulou R, Susini J. Biomedical applications of the ESRF synchrotron-based microspectroscopy platform. J Struct Biol. 2012; 177(2):248–258. S1047-8477(11)00352-2 [pii]. 10.1016/j.jsb.2011.12.006 [PubMed: 22182732]
13. Chen, S.; Flachenecker, C.; Lai, B.; Paunesku, T.; Roehrig, C.; Vonosinski, J.; Bolbat, M.; Maser, J.; Shu, D.; Finney, L.; Gleber, S.; Jin, Q.; Brister, K.; Jacobsen, C.; Vogt, S. Cambridge Journals. Woloschak G 2D/3D Trace Elemental Mapping of Frozen-hydrated Biomaterials Using the Bionanoprobe. Microscopy and Microanalysis, Phoenix, Az, 2012.
14. Matsuyama S, Mimura H, Yumoto H, Sano Y, Yamamura K, Yabashi M, Nishino Y, Tamasaku K, Ishikawa T, Yamauchi K. Development of scanning x-ray fluorescence microscope with spatial resolution of 30 nm using Kirkpatrick-Baez mirror optics. Rev Sci Instrum. 2006; 77(10) Artn 103102. 10.1063/1.2358699
15. Ryan C, Siddons D, Moorhead G, Kirkham R, Dunn P, Dragone A, De Geronimo G. Large detector array and real-time processing and elemental image projection of X-ray and proton microprobe fluorescence data. Nucl Instrum Methods Phys Res Sect B: Beam Interact Mater Atoms. 2007; 260:1–7.
16. Chen KG, Valencia JC, Lai B, Zhang G, Paterson JK, Rouzaud F, Berens W, Wincovitch SM, Garfield SH, Leapman RD, Hearing VJ, Gottesman MM. Melanosomal sequestration of cytotoxic

drugs contributes to the intractability of malignant melanomas. Proc Natl Acad Sci U S A. 2006; 103(26):9903–9907.10.1073/pnas.0600213103 [PubMed: 16777967]

17. Howells MR, Beetz T, Chapman HN, Cui C, Holton JM, Jacobsen CJ, Kirz J, Lima E, Marchesini S, Miao H, Sayre D, Shapiro DA, Spence JCH, Starodub D. An assessment of the resolution limitation due to radiation-damage in X-ray diffraction microscopy. Journal of Electron Spectroscopy and Related Phenomena. 2009; 170 (1–3):4–12. [PubMed: 20463854]
18. Schrag M, Dickson A, Jiffry A, Kirsch D, Vinters HV, Kirsch W. The effect of formalin fixation on the levels of brain transition metals in archived samples. Biometals. 2010; 23(6):1123–1127.10.1007/s10534-010-9359-4 [PubMed: 20582563]
19. James SA, Myers DE, de Jonge MD, Vogt S, Ryan CG, Sexton BA, Hoobin P, Paterson D, Howard DL, Mayo SC, Altissimo M, Moorhead GF, Wilkins SW. Quantitative comparison of preparation methodologies for X-ray fluorescence microscopy of brain tissue. Anal Bioanal Chem. 2011; 401(3):853–864.10.1007/s00216-011-4978-3 [PubMed: 21533642]
20. Matsuyama S, Shimura M, Fujii M, Maeshima K, Yumoto H, Mimura H, Sano Y, Yabashi M, Nishino Y, Tamasaku K, Ishizaka Y, Ishikawa T, Yamauchi K. Elemental mapping of frozen-hydrated cells with cryo-scanning X-ray fluorescence microscopy. X-Ray Spectrom. 2010; 39(4): 260–266.10.1002/xrs.1256
21. Lai, B.; Chen, S.; Bolbat, M.; Jin, Q.; Finney, L.; Brister, K.; Jacobsen, C.; Vogt, S. Cambridge Journals. A Flexible Cryojet-Cooled X-ray Fluorescence Microprobe: Initial Results. Microscopy and Microanalysis, Phoenix Az, 2012.
22. de Jonge MD, Vogt S. Hard X-ray fluorescence tomography--an emerging tool for structural visualization. Curr Opin Struct Biol. 2010; 20(5):606–614. S0959-440X(10)00137-5 [pii]. 10.1016/j.sbi.2010.09.002 [PubMed: 20934872]
23. de Jonge MD, Holzner C, Baines SB, Twining BS, Ignatyev K, Diaz J, Howard DL, Legnini D, Miceli A, McNulty I, Jacobsen CJ, Vogt S. Quantitative 3D elemental microtomography of Cyclotella meneghiniana at 400-nm resolution. Proc Natl Acad Sci U S A. 2010; 107(36):15676–15680. 1001469107 [pii]. 10.1073/pnas.1001469107 [PubMed: 20720164]
24. De Samber B, Silversmit G, De Schamphelaere K, Evens R, Schoonjans T, Vekemans B, Janssen C, Masschaele B, VanHoorebeke LS, zalók I, et al. Element-to-tissue correlation in biological samples determined by three-dimensional X-ray imaging methods. J Anal Atom Spectrom. 2010; 25:544–553.
25. Kim SA, Punshon T, Lanzirotti A, Li L, Alonso JM, Ecker JR, Kaplan J, Guerinot ML. Localization of iron in Arabidopsis seed requires the vacuolar membrane transporter VIT1. Science. 2006; 314(5803):1295–1298. 1132563 [pii]. 10.1126/science.1132563 [PubMed: 17082420]
26. McEwen BF, Downing KH, Glaeser RM. The relevance of dose-fractionation in tomography of radiation-sensitive specimens. Ultramicroscopy. 1995; 60 (3):357–373. [PubMed: 8525549]
27. Schlichting I, Miao J. Emerging opportunities in structural biology with X-ray free-electron lasers. Curr Opin Struct Biol. 201210.1016/j.sbi.2012.07.015
28. Boutet S, Lomb L, Williams GJ, Barends TR, Aquila A, Doak RB, Weierstall U, DePonte DP, Steinbrener J, Shoeman RL, Messerschmidt M, Barty A, White TA, Kassemeyer S, Kirian RA, Seibert MM, Montanez PA, Kenney C, Herbst R, Hart P, Pines J, Haller G, Gruner SM, Philipp HT, Tate MW, Hromalik M, Koerner LJ, van Bakel N, Morse J, Ghonsalves W, Arnlund D, Bogan MJ, Caleman C, Fromme R, Hampton CY, Hunter MS, Johansson LC, Katona G, Kupitz C, Liang M, Martin AV, Nass K, Redecke L, Stellato F, Timneanu N, Wang D, Zatsepin NA, Schafer D, Defever J, Neutze R, Fromme P, Spence JC, Chapman HN, Schlichting I. High-resolution protein structure determination by serial femtosecond crystallography. Science. 2012; 337(6092):362–364.10.1126/science.1217737 [PubMed: 22653729]
29. Seibert MM, Ekeberg T, Maia FR, Svenda M, Andreasson J, Jonsson O, Odic D, Iwan B, Rocker A, Westphal D, Hantke M, DePonte DP, Barty A, Schulz J, Gumprecht L, Coppola N, Aquila A, Liang M, White TA, Martin A, Caleman C, Stern S, Abergel C, Seltzer V, Claverie JM, Bostedt C, Bozek JD, Boutet S, Miahnahri AA, Messerschmidt M, Krzywinski J, Williams G, Hodgson KO, Bogan MJ, Hampton CY, Sierra RG, Starodub D, Andersson I, Bajt S, Barthelmess M, Spence JC, Fromme P, Weierstall U, Kirian R, Hunter M, Doak RB, Marchesini S, Hau-Riege SP, Frank M, Shoeman RL, Lomb L, Epp SW, Hartmann R, Rolles D, Rudenko A, Schmidt C, Foucar L,

Kimmel N, Holl P, Rudek B, Erk B, Homke A, Reich C, Pietschner D, Weidenspointner G, Struder L, Hauser G, Gorke H, Ullrich J, Schlichting I, Herrmann S, Schaller G, Schopper F, Soltau H, Kuhnel KU, Andritschke R, Schroter CD, Krasniqi F, Bott M, Schorb S, Rupp D, Adolph M, Gorkhover T, Hirsemann H, Potdevin G, Graafsma H, Nilsson B, Chapman HN, Hajdu J. Single mimivirus particles intercepted and imaged with an X-ray laser. Nature. 2011; 470(7332): 78–81.10.1038/nature09748 [PubMed: 21293374]

30. Vogt S. Maps: A set of software tools for analysis and visualization of 3D X-ray fluorescent datasets. Journal De Physique IV. 2003; 104:635–638.
31. Solé VA, Papillon E, Cotte M, Walter P, Susini J. A multiplatform code for the analysis of energy-dispersive X-ray fluorescence spectra. Spectrochim Acta Part B. 2007; 62:63–68. doi: http://dx.doi.org/10.1016/j.sab.2006.12.002.
32. de Jonge MD, Hornberger B, Holzner C, Legnini D, Paterson D, McNulty I, Jacobsen C, Vogt S. Quantitative phase imaging with a scanning transmission x-ray microscope. Phys Rev Lett. 2008; 100 (16):163902. [PubMed: 18518198]
33. Hornberger B, de Jonge MD, Feser M, Holl P, Holzner C, Jacobsen C, Legnini D, Paterson D, Rehak P, Struder L, Vogt S. Differential phase contrast with a segmented detector in a scanning X-ray microprobe. J Synchrotron Radiat. 2008; 15(Pt 4):355–362. S0909049508008509 [pii]. 10.1107/S0909049508008509 [PubMed: 18552427]
34. Holzner C, Feser M, Vogt S, Hornberger B, Baines SB, Jacobsen C. Zernike phase contrast in scanning microscopy with X-rays. Nat Phys. 2010; 6 (11):883–887. [PubMed: 21544232]
35. Leskovjan AC, Kretlow A, Lanzirotti A, Barrea R, Vogt S, Miller LM. Increased brain iron coincides with early plaque formation in a mouse model of Alzheimer's disease. Neuroimage. 2011; 55(1):32–38.10.1016/j.neuroimage.2010.11.073 [PubMed: 21126592]
36. Leskovjan AC, Kretlow A, Miller LM. Fourier transform infrared imaging showing reduced unsaturated lipid content in the hippocampus of a mouse model of Alzheimer's disease. Anal Chem. 2010; 82(7):2711–2716.10.1021/ac1002728 [PubMed: 20187625]
37. Leskovjan AC, Lanzirotti A, Miller LM. Amyloid plaques in PSAPP mice bind less metal than plaques in human Alzheimer's disease. Neuroimage. 2009; 47(4):1215–1220.10.1016/j.neuroimage.2009.05.063 [PubMed: 19481608]
38. Miller LM, Wang Q, Telivala TP, Smith RJ, Lanzirotti A, Miklossy J. Synchrotron-based infrared and X-ray imaging shows focalized accumulation of Cu and Zn co-localized with beta-amyloid deposits in Alzheimer's disease. J Struct Biol. 2006; 155(1):30–37. S1047-8477(05)00196-6 [pii]. 10.1016/j.jsb.2005.09.004 [PubMed: 16325427]
39. Miller LM, Wang Q, Smith RJ, Zhong H, Elliott D, Warren J. A new sample substrate for imaging and correlating organic and trace metal composition in biological cells and tissues. Anal Bioanal Chem. 2007; 387(5):1705–1715.10.1007/s00216-006-0879-2 [PubMed: 17115141]
40. Takizawa T, Suzuki K, Robinson JM. Correlative microscopy using FluoroNanogold on ultrathin cryosections. Proof of principle. J Histochem Cytochem. 1998; 46 (10):1097–1102. [PubMed: 9742065]
41. Takizawa T, Robinson JM. FluoroNanogold is a bifunctional immunoprobe for correlative fluorescence and electron microscopy. J Histochem Cytochem. 2000; 48 (4):481–486. [PubMed: 10727289]
42. Endres PJ, Macrenaris KW, Vogt S, Allen MJ, Meade TJ. Quantitative imaging of cell-permeable magnetic resonance contrast agents using x-ray fluorescence. Mol Imaging. 2006; 5 (4):485–497. [PubMed: 17150161]
43. Endres PJ, MacRenaris KW, Vogt S, Meade TJ. Cell-permeable MR contrast agents with increased intracellular retention. Bioconjug Chem. 2008; 19(10):2049–2059.10.1021/bc8002919 [PubMed: 18803414]
44. Endres PJ, Paunesku T, Vogt S, Meade TJ, Woloschak GE. DNA-TiO2 nanoconjugates labeled with magnetic resonance contrast agents. J Am Chem Soc. 2007; 129(51):15760–15761.10.1021/ja0772389 [PubMed: 18047347]
45. Paunesku T, Ke T, Dharmakumar R, Mascheri N, Wu A, Lai B, Vogt S, Maser J, Thurn K, Szolc-Kowalska B, Larson A, Bergan RC, Omary R, Li D, Lu ZR, Woloschak GE. Gadolinium-conjugated TiO2-DNA oligonucleotide nanoconjugates show prolonged intracellular retention

period and T1-weighted contrast enhancement in magnetic resonance images. Nanomedicine : nanotechnology, biology, and medicine. 2008; 4(3):201–207. S1549-9634(08)00046-4 [pii]. 10.1016/j.nano.2008.04.004

46. Paunesku T, Vogt S, Lai B, Maser J, Stojicevic N, Thurn KT, Osipo C, Liu H, Legnini D, Wang Z, Lee C, Woloschak GE. Intracellular distribution of TiO2-DNA oligonucleotide nanoconjugates directed to nucleolus and mitochondria indicates sequence specificity. Nano Lett. 2007; 7(3):596–601.10.1021/nl0624723 [PubMed: 17274661]
47. Corezzi S, Urbanelli L, Cloetens P, Emiliani C, Helfen L, Bohic S, Elisei F, Fioretto D. Synchrotron-based X-ray fluorescence imaging of human cells labeled with CdSe quantum dots. Anal Biochem. 2009; 388(1):33–39. S0003-2697(09)00072-4 [pii]. 10.1016/j.ab.2009.01.044 [PubMed: 19454226]
48. Ornatsky O, Bandura D, Baranov V, Nitz M, Winnik MA, Tanner S. Highly multiparametric analysis by mass cytometry. J Immunol Methods. 2010; 361(1–2):1–20. S0022-1759(10)00198-5 [pii]. 10.1016/j.jim.2010.07.002 [PubMed: 20655312]
49. Dodani SC, Domaille DW, Nam CI, Miller EW, Finney LA, Vogt S, Chang CJ. Calcium-dependent copper redistributions in neuronal cells revealed by a fluorescent copper sensor and X-ray fluorescence microscopy. Proc Natl Acad Sci U S A. 2011; 108(15):5980–5985. 1009932108 [pii]. 10.1073/pnas.1009932108 [PubMed: 21444780]
50. Domaille DW, Zeng L, Chang CJ. Visualizing ascorbate-triggered release of labile copper within living cells using a ratiometric fluorescent sensor. J Am Chem Soc. 2010; 132(4):1194–1195.10.1021/ja907778b [PubMed: 20052977]
51. Miller EW, Zeng L, Domaille DW, Chang CJ. Preparation and use of Coppersensor-1, a synthetic fluorophore for live-cell copper imaging. Nat Protoc. 2006; 1(2):824–827. nprot.2006.140 [pii]. 10.1038/nprot.2006.140 [PubMed: 17406313]
52. Zeng L, Miller EW, Pralle A, Isacoff EY, Chang CJ. A selective turn-on fluorescent sensor for imaging copper in living cells. J Am Chem Soc. 2006; 128(1):10–11.10.1021/ja055064u [PubMed: 16390096]
53. Taki M, Iyoshi S, Ojida A, Hamachi I, Yamamoto Y. Development of highly sensitive fluorescent probes for detection of intracellular copper(I) in living systems. J Am Chem Soc. 2010; 132(17): 5938–5939.10.1021/ja100714p [PubMed: 20377254]
54. Hirayama T, Van de Bittner GC, Gray LW, Lutsenko S, Chang CJ. Near-infrared fluorescent sensor for in vivo copper imaging in a murine Wilson disease model. Proc Natl Acad Sci U S A. 2012; 109(7):2228–2233. 1113729109 [pii]. 10.1073/pnas.1113729109 [PubMed: 22308360]
55. Rurack K, Resch-Genger U. Rigidization, preorientation and electronic decoupling--the 'magic triangle' for the design of highly efficient fluorescent sensors and switches. Chem Soc Rev. 2002; 31 (2):116–127. [PubMed: 12109205]
56. Chaudhry AF, Verma M, Morgan MT, Henary MM, Siegel N, Hales JM, Perry JW, Fahrni CJ. Kinetically controlled photoinduced electron transfer switching in Cu(I)-responsive fluorescent probes. J Am Chem Soc. 2010; 132(2):737–747.10.1021/ja908326z [PubMed: 20020716]
57. Verma M, Chaudhry AF, Morgan MT, Fahrni CJ. Electronically tuned 1,3,5-triarylpyrazolines as Cu(I)-selective fluorescent probes. Org Biomol Chem. 2010; 8(2):363–370.10.1039/b918311f [PubMed: 20066271]
58. Rubino JT, Franz KJ. Coordination chemistry of copper proteins: how nature handles a toxic cargo for essential function. J Inorg Biochem. 2012; 107(1):129–143. S0162-0134(11)00372-2 [pii]. 10.1016/j.jinorgbio.2011.11.024 [PubMed: 22204943]
59. Bremner I. Manifestations of copper excess. Am J Clin Nutr. 1998; 67 (5 Suppl):1069S–1073S. [PubMed: 9587154]
60. O'Halloran TV, Culotta VC. Metallochaperones, an intracellular shuttle service for metal ions. J Biol Chem. 2000; 275(33):25057–25060.10.1074/jbc.R000006200 R000006200 [pii] [PubMed: 10816601]
61. Rae TD, Schmidt PJ, Pufahl RA, Culotta VC, O'Halloran TV. Undetectable intracellular free copper: the requirement of a copper chaperone for superoxide dismutase. Science. 1999; 284 (5415):805–808. [PubMed: 10221913]

62. Tanzi RE, Petrukhin K, Chernov I, Pellequer JL, Wasco W, Ross B, Romano DM, Parano E, Pavone L, Brzustowicz LM, et al. The Wilson disease gene is a copper transporting ATPase with homology to the Menkes disease gene. Nat Genet. 1993; 5 (4):344–350. [PubMed: 8298641]
63. Mercer JF, Livingston J, Hall B, Paynter JA, Begy C, Chandrasekharappa S, Lockhart P, Grimes A, Bhave M, Siemieniak D, et al. Isolation of a partial candidate gene for Menkes disease by positional cloning. Nat Genet. 1993; 3 (1):20–25. [PubMed: 8490647]
64. Issue T. Metals in Neurodegenerative Disease. Metallomics. 2011; 3 (3):217–304.
65. Banci L, Bertini I, Cantini F, Ciofi-Baffoni S. Cellular copper distribution: a mechanistic systems biology approach. Cell Mol Life Sci. 2010; 67(15):2563–2589.10.1007/s00018-010-0330-x [PubMed: 20333435]
66. Kim BE, Nevitt T, Thiele DJ. Mechanisms for copper acquisition, distribution and regulation. Nat Chem Biol. 2008; 4(3):176–185. nchembio.72 [pii]. 10.1038/nchembio.72 [PubMed: 18277979]
67. Wang Y, Hodgkinson V, Zhu S, Weisman GA, Petris MJ. Advances in the understanding of mammalian copper transporters. Adv Nutr. 2011; 2(2):129–137.10.3945/an.110.000273 000273 [pii] [PubMed: 22332042]
68. Collins JF, Prohaska JR, Knutson MD. Metabolic crossroads of iron and copper. Nutr Rev. 2010; 68(3):133–147. NURE271 [pii]. 10.1111/j.1753-4887.2010.00271.x [PubMed: 20384844]
69. Bull PC, Thomas GR, Rommens JM, Forbes JR, Cox DW. The Wilson disease gene is a putative copper transporting P-type ATPase similar to the Menkes gene. Nat Genet. 1993; 5 (4):327–337. [PubMed: 8298639]
70. Schushan M, Bhattacharjee A, Ben-Tal N, Lutsenko S. A structural model of the copper ATPase ATP7B to facilitate analysis of Wilson disease-causing mutations and studies of the transport mechanism. Metallomics. 201210.1039/c2mt20025b
71. Lutsenko S, Barnes NL, Bartee MY, Dmitriev OY. Function and regulation of human copper-transporting ATPases. Physiol Rev. 2007; 87 (3):1011–1046. [PubMed: 17615395]
72. Guo Y, Nyasae L, Braiterman LT, Hubbard AL. NH2-terminal signals in ATP7B Cu-ATPase mediate its Cu-dependent anterograde traffic in polarized hepatic cells. Am J Physiol Gastrointest Liver Physiol. 2005; 289(5):G904–916. 00262.2005 [pii]. 10.1152/ajpgi.00262.2005 [PubMed: 15994426]
73. Cater MA, La Fontaine S, Shield K, Deal Y, Mercer JF. ATP7B mediates vesicular sequestration of copper: insight into biliary copper excretion. Gastroenterology. 2006; 130(2):493–506. S0016-5085(05)02235-3 [pii]. 10.1053/j.gastro.2005.10.054 [PubMed: 16472602]
74. Scott LD. Copper toxicity in primary biliary cirrhosis. Gastroenterology. 1978; 74 (2 Pt 1):333–334. [PubMed: 620907]
75. Brewer GJ. Wilson disease and canine copper toxicosis. Am J Clin Nutr. 1998; 67 (5 Suppl): 1087S–1090S. [PubMed: 9587157]
76. Brewer GJ, Yuzbasiyan-Gurkan V. Wilson disease. Medicine (Baltimore). 1992; 71 (3):139–164. [PubMed: 1635439]
77. Buiakova OI, Xu J, Lutsenko S, Zeitlin S, Das K, Das S, Ross BM, Mekios C, Scheinberg IH, Gilliam TC. Null mutation of the murine ATP7B (Wilson disease) gene results in intracellular copper accumulation and late-onset hepatic nodular transformation. Hum Mol Genet. 1999; 8 (9): 1665–1671. [PubMed: 10441329]
78. Huster D, Finegold MJ, Morgan CT, Burkhead JL, Nixon R, Vanderwerf SM, Gilliam CT, Lutsenko S. Consequences of copper accumulation in the livers of the atp7b−/− (Wilson disease gene) knockout mice. Am J Pathol. 2006; 168 (2):423–434. [PubMed: 16436657]
79. Huster D, Purnat TD, Burkhead JL, Ralle M, Fiehn O, Stuckert F, Olson NE, Teupser D, Lutsenko S. High copper selectively alters lipid metabolism and cell cycle machinery in the mouse model of Wilson disease. J Biol Chem. 2007; 282 (11):8343–8355. [PubMed: 17205981]
80. Chelly J, Tumer Z, Tonnesen T, Petterson A, Ishikawa-Brush Y, Tommerup N, Horn N, Monaco AP. Isolation of a candidate gene for Menkes disease that encodes a potential heavy metal binding protein. Nat Genet. 1993; 3 (1):14–19. [PubMed: 8490646]
81. Nyasae L, Bustos R, Braiterman L, Eipper B, Hubbard A. Dynamics of endogenous ATP7A (Menkes protein) in intestinal epithelial cells: copper-dependent redistribution between two

intracellular sites. Am J Physiol Gastrointest Liver Physiol. 2007; 292(4):G1181–1194. 00472.2006 [pii]. 10.1152/ajpgi.00472.2006 [PubMed: 17158254]

82. Goldfischer S, Sternlieb I. Changes in the distribution of hepatic copper in relation to the progression of Wilson's disease (hepatolenticular degeneration). Am J Pathol. 1968; 53 (6):883–901. [PubMed: 4177374]
83. Sternlieb I. Evolution of the hepatic lesion in Wilson's disease (hepatolenticular degeneration). Prog Liver Dis. 1972; 4:511–525. [PubMed: 4569009]
84. Goldfischer S. Demonstration of copper and acid phosphatase activity in hepatocyte lysosomes in experimental copper toxicity. Nature. 1967; 215 (5096):74–75. [PubMed: 4167884]
85. Haywood S, Loughran M, Batt RM. Copper toxicosis and tolerance in the rat. III. Intracellular localization of copper in the liver and kidney. Exp Mol Pathol. 1985; 43 (2):209–219. [PubMed: 4043340]
86. Scheinberg, IH.; Sternlieb, I. Major Problems in Internal Medicine. Vol. XXIII. W.B. Saunders Company; 1984. Wilson's Disease.
87. Ralle M, Huster D, Vogt S, Schirrmeister W, Burkhead JL, Capps TR, Gray L, Lai B, Maryon E, Lutsenko S. Wilson's disease at a single cell level:intracellular copper trafficking activates compartment-specific responses in hepatocytes. J Biol Chem. 2010 M110.114447 [pii]. 10.1074/jbc.M110.114447
88. Peng F, Lutsenko S, Sun X, Muzik O. Positron emission tomography of copper metabolism in the Atp7b(−)/(−) knock-out mouse model of Wilson's disease. Mol Imaging Biol. 2012; 14(1):70–78.10.1007/s11307-011-0476-4 [PubMed: 21327972]
89. Hamza I, Schaefer M, Klomp LW, Gitlin JD. Interaction of the copper chaperone HAH1 with the Wilson disease protein is essential for copper homeostasis. Proc Natl Acad Sci U S A. 1999; 96 (23):13363–13368. [PubMed: 10557326]
90. Hamza I, Prohaska J, Gitlin JD. Essential role for Atox1 in the copper-mediated intracellular trafficking of the Menkes ATPase. Proc Natl Acad Sci U S A. 2003; 100(3):1215–1220.10.1073/pnas.0336230100 [PubMed: 12538877]
91. Walker JM, Tsivkovskii R, Lutsenko S. Metallochaperone Atox1 transfers copper to the NH2-terminal domain of the Wilson's disease protein and regulates its catalytic activity. J Biol Chem. 2002; 277(31):27953–27959.10.1074/jbc.M203845200 [PubMed: 12029094]
92. Ralle M, Cooper MJ, Lutsenko S, Blackburn NJ. The Menkes Disease Protein Binds Copper via Novel 2-Coordinate Cu(I)-Cysteinates in the N-Terminal Domain. J Am Chem Soc. 1998; 120 (51):13525–13526.
93. Ralle M, Lutsenko S, Blackburn NJ. X-ray absorption spectroscopy of the copper chaperone HAH1 reveals a linear two-coordinate Cu(I) center capable of adduct formation with exogenous thiols and phosphines. J Biol Chem. 2003; 278 (25):23163–23170. [PubMed: 12686548]
94. Ralle M, Lutsenko S, Blackburn NJ. Copper transfer to the N-terminal domain of the Wilson disease protein (ATP7B): X-ray absorption spectroscopy of reconstituted and chaperone-loaded metal binding domains and their interaction with exogenous ligands. J Inorg Biochem. 2004; 98 (5):765–774. [PubMed: 15134922]
95. McRae R, Lai B, Fahrni CJ. Copper redistribution in Atox1-deficient mouse fibroblast cells. J Biol Inorg Chem. 2010; 15(1):99–105.10.1007/s00775-009-0598-1 [PubMed: 19865834]
96. Goodman L. Alzheimer's disease; a clinico-pathologic analysis of twenty-three cases with a theory on pathogenesis. The Journal of nervous and mental disease. 1953; 118 (2):97–130. [PubMed: 13109530]
97. Bonda DJ, Lee HG, Blair JA, Zhu X, Perry G, Smith MA. Role of metal dyshomeostasis in Alzheimer's disease. Metallomics. 2011; 3(3):267–270.10.1039/c0mt00074d [PubMed: 21298161]
98. Hung YH, Bush AI, Cherny RA. Copper in the brain and Alzheimer's disease. J Biol Inorg Chem. 2010; 15(1):61–76.10.1007/s00775-009-0600-y [PubMed: 19862561]
99. Atwood CS, Perry G, Zeng H, Kato Y, Jones WD, Ling KQ, Huang X, Moir RD, Wang D, Sayre LM, Smith MA, Chen SG, Bush AI. Copper mediates dityrosine cross-linking of Alzheimer's amyloid-beta. Biochemistry. 2004; 43(2):560–568.10.1021/bi0358824 [PubMed: 14717612]
100. Huang X, Atwood CS, Moir RD, Hartshorn MA, Tanzi RE, Bush AI. Trace metal contamination initiates the apparent auto-aggregation, amyloidosis, and oligomerization of Alzheimer's Abeta

peptides. J Biol Inorg Chem. 2004; 9(8):954–960.10.1007/s00775-004-0602-8 [PubMed: 15578276]

101. Zhu X, Su B, Wang X, Smith MA, Perry G. Causes of oxidative stress in Alzheimer disease. Cell Mol Life Sci. 2007; 64(17):2202–2210.10.1007/s00018-007-7218-4 [PubMed: 17605000]
102. Schrag M, Mueller C, Oyoyo U, Smith MA, Kirsch WM. Iron, zinc and copper in the Alzheimer's disease brain: a quantitative meta-analysis. Some insight on the influence of citation bias on scientific opinion. Prog Neurobiol. 2011; 94(3):296–306.10.1016/j.pneurobio.2011.05.001 [PubMed: 21600264]
103. Bush AI. Metals and neuroscience. Curr Opin Chem Biol. 2000; 4(2):184–191. S1367-5931(99)00073-3 [pii]. [PubMed: 10742195]
104. Tougu V, Tiiman A, Palumaa P. Interactions of Zn(II) and Cu(II) ions with Alzheimer's amyloid-beta peptide. Metal ion binding, contribution to fibrillization and toxicity. Metallomics. 2011; 3(3):250–261.10.1039/c0mt00073f [PubMed: 21359283]
105. Lovell MA, Robertson JD, Teesdale WJ, Campbell JL, Markesbery WR. Copper, iron and zinc in Alzheimer's disease senile plaques. Journal of the neurological sciences. 1998; 158 (1):47–52. [PubMed: 9667777]
106. Hutchinson RW, Cox AG, McLeod CW, Marshall PS, Harper A, Dawson EL, Howlett DR. Imaging and spatial distribution of beta-amyloid peptide and metal ions in Alzheimer's plaques by laser ablation-inductively coupled plasma-mass spectrometry. Anal Biochem. 2005; 346(2):225–233.10.1016/j.ab.2005.08.024 [PubMed: 16214103]
107. Rajendran R, Minqin R, Ynsa MD, Casadesus G, Smith MA, Perry G, Halliwell B, Watt F. A novel approach to the identification and quantitative elemental analysis of amyloid deposits--insights into the pathology of Alzheimer's disease. Biochem Biophys Res Commun. 2009; 382(1):91–95.10.1016/j.bbrc.2009.02.136 [PubMed: 19258010]
108. Wang H, Wang M, Wang B, Li M, Chen H, Yu X, Zhao Y, Feng W, Chai Z. The distribution profile and oxidation states of biometals in APP transgenic mouse brain: dyshomeostasis with age and as a function of the development of Alzheimer's disease. Metallomics. 2012; 4(3):289–296.10.1039/c2mt00104g [PubMed: 22301945]

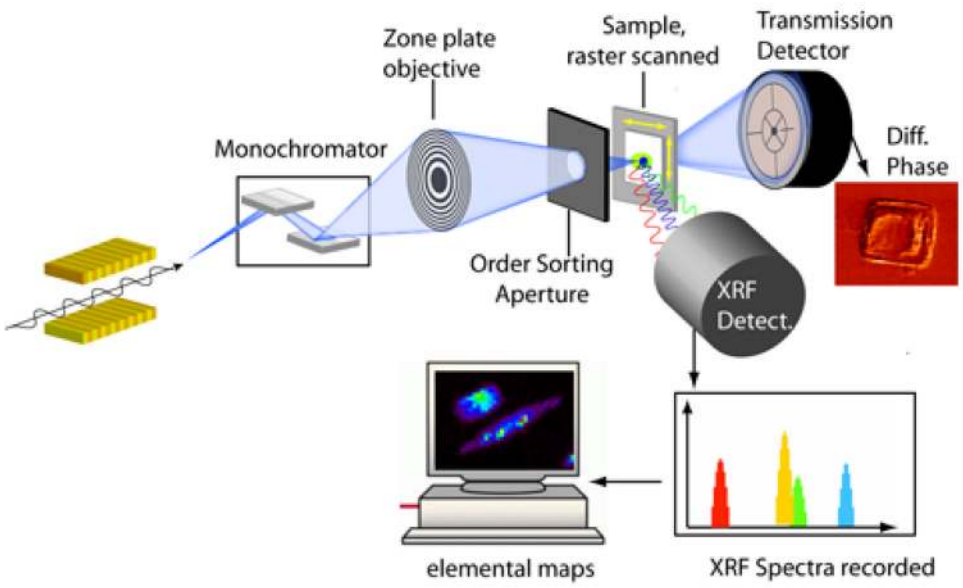

Fig. 1.
Scheme illustrating the experimental setup for XFM experiments

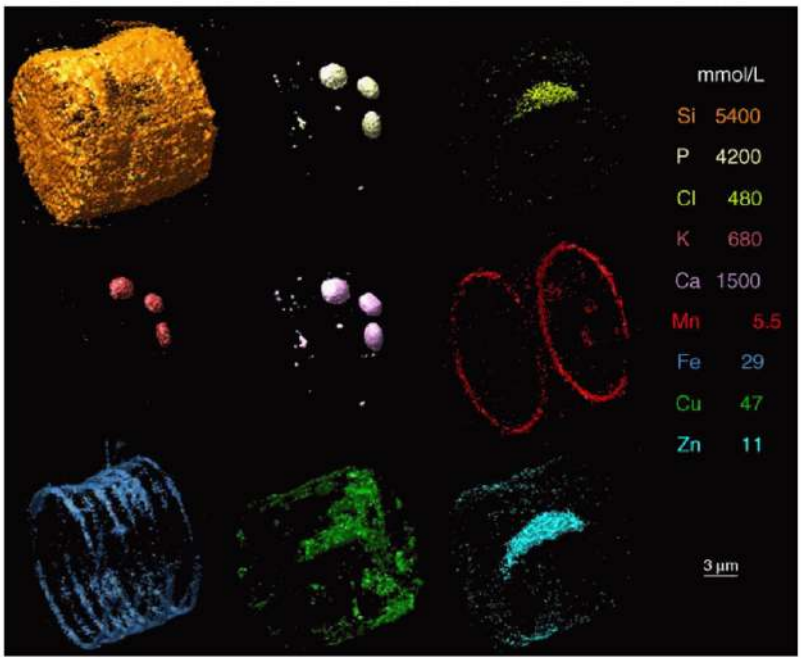

Fig. 2.
Tomographic visualization of elemental distributions in Cyclotella meneghiniana. Iso surface concentrations used for the display are indicated in mmol/l. Mn and Fe rings correlate with specific locations in the Si frustule. The total elemental content spans several orders of magnitude [reproduced with permission from [23]]

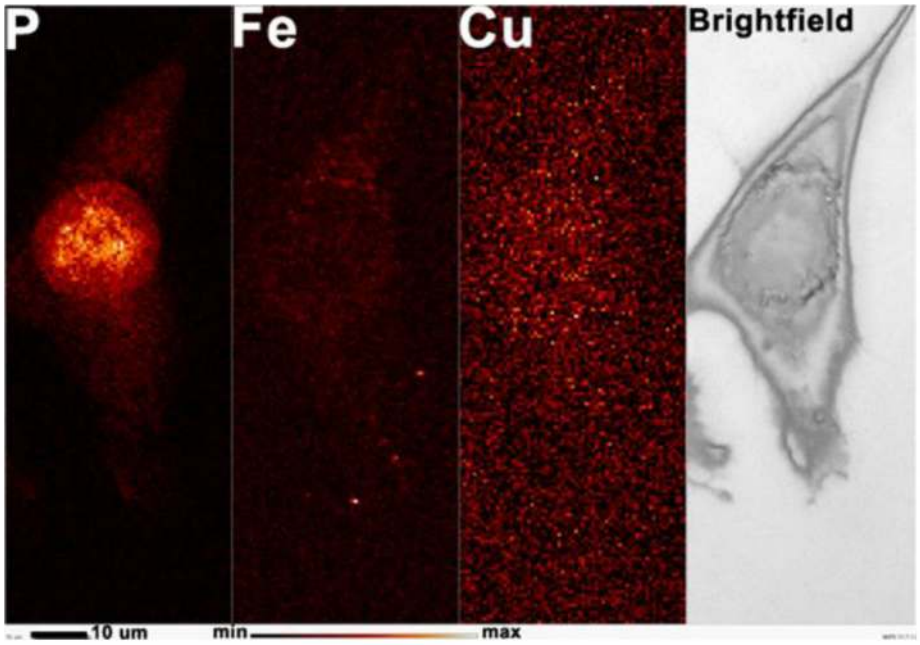

Fig. 3.

Phosphorous (P), iron (Fe), and copper (Cu) XFM map and bright field image for a human fibroblast. The nucleus is clearly visible as the brightest (i.e. most concentrated) area in the P elemental map. The bar at the bottom of the image illustrates the false color display for the concentration range of the elements (red temperature scale)

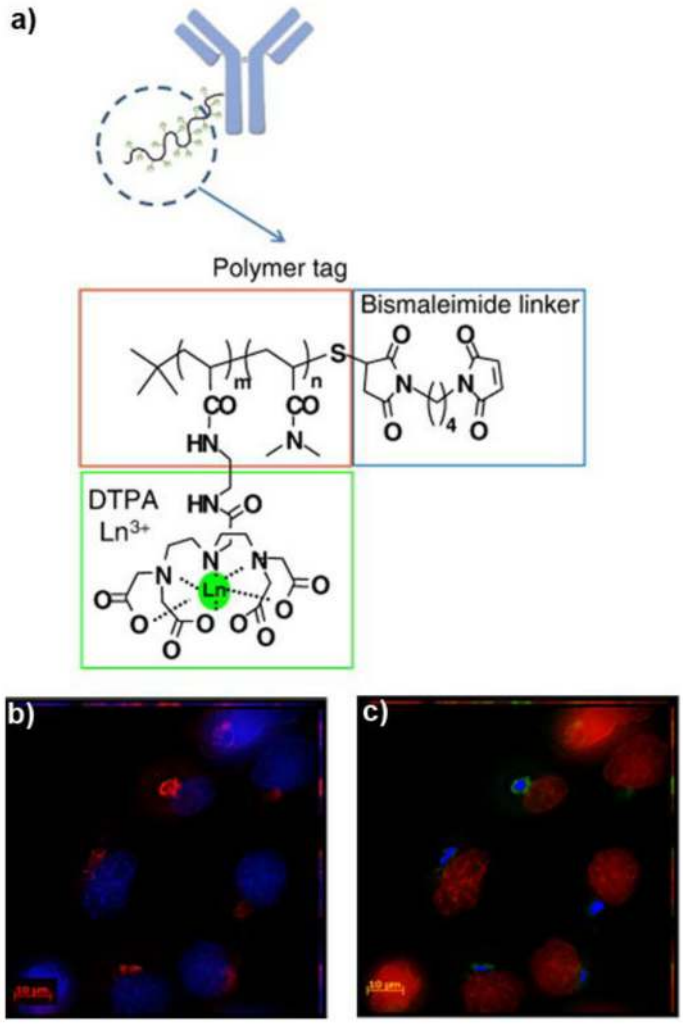

Fig. 4.

Illustration of the use of lanthanide conjugates as potential organelle markers in XFM. a) A schematic of the chemical structure of a lanthanide containing polymer conjugated to a primary antibody. b) Immunofluorescent image of human fibroblasts labeled with DAPI (blue) depicting the nuclei and anti-TG46 to outline the trans-Golgi network (TGN, red). No information about the localization of copper is available. c) A fictional XFM image illustrating the potential use of Pr-tagged anti-TG46. The elemental distribution for P (red) outlines the nuclei while Cu (blue) and Pr (green) are hypothetically co-localized in the TGN. 4a) was reproduced with permission from [48]